Supporting Information:

Multiexciton Absorption Cross Sections of CdSe Quantum Dots Determined by Ultrafast Spectroscopy

Nils Lenngren,[†,‡] Tommy Garting,[†,‡] Kaibo Zheng,[†] Mohamed Abdellah,[†,¶]

Noëlle Lascoux,[†,§] Fei Ma,[†,‖] Arkady Yartsev,[†] Karel Žídek,[†] and Tõnu Pullerits[*,†]

Department of Chemical Physics, Lund University, Box 124, 221 00 Lund, Sweden

E-mail: tonu.pullerits@chemphys.lu.se

[*] To whom correspondence should be addressed
[†] Lund University
[‡] Contributed equally to this work
[¶] Department of Chemistry, Qena Faculty of Science, South Valley University, Qena 83523, Egypt
[§] Current address: ILM, Université Claude Bernard Lyon 1, France
[‖] Current address: Biophysics of Photosynthesis Division, University of Amsterdam, The Netherlands

1. Multiexponential fits

Table S1: The excitation intensities used for each sample, expressed as a sample-specific reference intensity I_0 times a factor.

Sample	I_0 (photons/(pulse·cm^2))	Factors			
L0	$3.08 \cdot 10^{13}$	1	3.8	11.6	45.8
S0	$1.07 \cdot 10^{14}$	1	12.0	25.0	55.0
S5 at 540 nm	$1.00 \cdot 10^{14}$	1	13.0	55.0	126.3
S5 at 575 nm	$2.32 \cdot 10^{13}$	1	22.0	98.0	210.0
S300	$1.00 \cdot 10^{14}$	1	33.0	51.8	116.3

The pump intensities as given in Table S1 gave rise to the signals shown in Fig. 2 and Fig. S1. The signals shown here were measured in a static cuvette, since test runs with static and rotating cuvettes had shown the same signal. The initial amplitudes corresponding to the initial signal from each exciton level and the corresponding decay lifetimes were extracted by fitting one component at a time from the slowest to the fastest by fits in the appropriate time region. All measurements of each sample were fitted globally, except for the slowest component where only the highest-intensity trace was fitted due to high noise levels in the other traces. When fitting the faster components, all previously fitted components were included as fixed. Five exponentials were used. The excitation pulse was modeled by convoluting the exponentials with a Gaussian. The extracted amplitudes from the L0 sample at 592 nm are shown as an example in Table S2, and all lifetimes in Table S3.

A constant pre-pump signal with the same sign as the transient was seen in all measurements. It was subtracted before the fitting. The possibility that it represents a long-lived signal from charged QDs (recombining on the same timescale as the repetition rate of the laser, i.e. 1 ms) was investigated, but in the absence of more detailed measurements of the charging specifically it is hard to calculate reliably how much this will shift the transient signal, and fitting including an estimate of the charging effect did not lead to markedly different results from the simple subtraction approach, which is why we do not include it here.

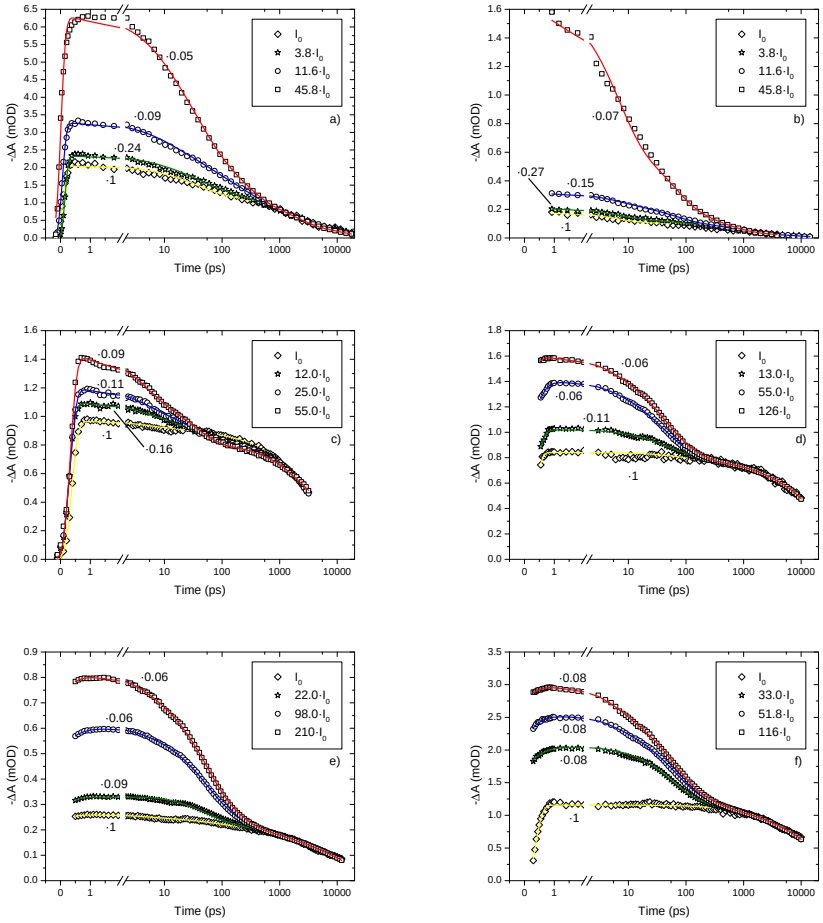

Figure S1: TA kinetics for the four pump intensities, normalized at times longer than 6 ns, and fits. The normalization factors are given next to each trace. a) L0, probed at 592 nm. b) L0, probed at 550 nm. c) S0, probed at 526 nm. d) S5, probed at 540 nm. e) S5, probed at 575 nm. f) S300, probed at 540 nm.

Table S2: Amplitudes retrieved from the five-exponential fits seen in Figure 2. Note that the y-axis in the figure shows $-\Delta A$.

Intensity	$A_{1,\alpha}$	$A_{1,\beta}$	A_2	A_3	A_4
$1.0 \cdot I_0$	$-4.18 \cdot 10^{-4}$	$-7.22 \cdot 10^{-4}$	$-2.86 \cdot 10^{-4}$	$-2.65 \cdot 10^{-4}$	$-3.91 \cdot 10^{-4}$
$3.8 \cdot I_0$	$-1.74 \cdot 10^{-3}$	$-3.01 \cdot 10^{-3}$	$-2.03 \cdot 10^{-3}$	$-1.08 \cdot 10^{-3}$	$-2.01 \cdot 10^{-3}$
$11.6 \cdot I_0$	$-4.42 \cdot 10^{-3}$	$-7.62 \cdot 10^{-3}$	$-1.08 \cdot 10^{-2}$	$-4.90 \cdot 10^{-3}$	$-7.20 \cdot 10^{-3}$
$45.8 \cdot I_0$	$-8.45 \cdot 10^{-3}$	$-1.46 \cdot 10^{-2}$	$-3.18 \cdot 10^{-2}$	$-5.08 \cdot 10^{-2}$	$-2.22 \cdot 10^{-2}$

Table S3: Lifetimes τ_N of the N-excitons.

Sample	$\tau_{1,\alpha}$ (ns)	$\tau_{1,\beta}$ (ns)	τ_2 (ps)	τ_3 (ps)	τ_4 (ps)
L0 at 592 nm	14	1.7	210	39	9.2
L0 at 550 nm	11	0.85	320	60	6.4
S0	18	1.6	690	33	4.0
S5 at 575 nm	17	1.5	160	44	9.2
S5 at 540 nm	25	1.7	100	32	4.3
S300	22	1.6	230	56	11

2. Calculations of the initial population distribution

Table S4: Average number of excitons at I_0 per QD $\langle N \rangle_0$, and absorption cross section at the pump wavelength σ_{abs}, calculated from the highest, average and lowest values of ΔA_0 at each intensity.

Sample	High ΔA_0		Average ΔA_0		Low ΔA_0	
	$\langle N \rangle_0$	σ_{abs} (Å^2)	$\langle N \rangle_0$	σ_{abs} (Å^2)	$\langle N \rangle_0$	σ_{abs} (Å^2)
L0 at 592 nm	0.062	17	0.065	18	0.069	19
L0 at 550 nm	0.058	16	0.088	24	0.13	34
S0	0.079	7.4	0.075	7.0	0.068	6.4
S5 at 575 nm	0.049	21	0.046	20	0.045	19
S5 at 540 nm	0.059	5.9	0.059	5.9	0.059	5.9
S300	0.11	11	0.11	11	0.11	11

Table S5: Values of σ_{abs} in Å^2 calculated from the average values of ΔA_0, with errors estimated from fits to the highest and lowest values. The red edge is 592 nm for sample L0 and 575 nm for sample S5. The peak is 540 nm for sample S5 and S300. The blue edge is 550 nm for sample L0 and 526 nm for sample S0.

Sample	Probed at		
	Blue edge	Peak	Red edge
L0	24 ± 10		17.8 ± 0.6
S0	7.0 ± 0.6		
S5		5.90 ± 0.02	20 ± 1
S300		10.9 ± 0.3	

The signals at long timescales were rescaled to $t = 0$ and fitted to Eq. 3. The results are shown in Fig. 3, Fig. S2, Table S4 and Table S5. The obtained cross sections can be compared by the expressions given by Yu et al.[1] and Leatherdale et al.[2] All results agree with the predictions within a factor of 2, except for the core–shell samples where the Leatherdale formula generally underestimates the cross section, and our cross section of sample S5 at the band edge, which is more than 3 times larger than both the Yu prediction and the corresponding result away from the band edge. The anomalous core–shell predictions can be explained by the fact that Leatherdale et al. predict the cross section at 350 nm for core QDs only, and the shape of core–shell QD absorption spectra—which is used to recalculate to our pump wavelengths—differs significantly from the shape of core QD absorption spectra. The

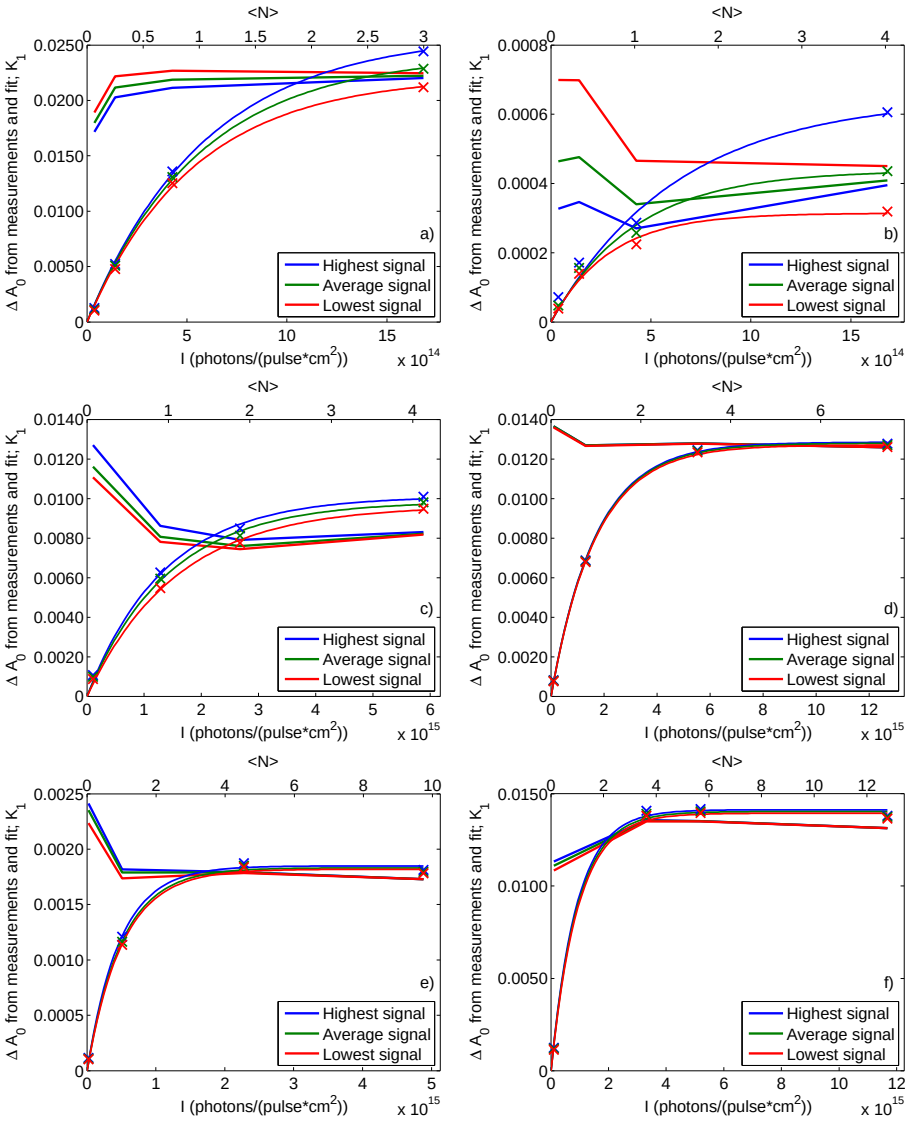

Figure S2: Maximum, average and minimum TA signal (crosses) ΔA_0 rescaled from $t > 6$ ns (see Fig. S1) as a function of excitation intensity (lower axis) and average number of excitons per quantum dots (upper axis). Fits based on the maximum and minimum provide the maximum and minimum values for $\langle N \rangle_0$ according to Eq. 3, and a fit to the average values provides the $\langle N \rangle_0$ that best represents the entire data set. Also included are the maximum signals from the 1-excitons K_1 obtained from analyses of the kinetics. The averaged $\langle N \rangle$ leads to the best consistency with the corresponding K_1 values, both represented by green lines. The low-$\langle N \rangle$ fit is clearly inconsistent with the corresponding K_1 (both represented by blue lines). The accuracy of the K_1 values at I_0 is affected by large errors in the measurements of low intensities. a) L0, probed at 592 nm. b) L0, probed at 550 nm. c) S0, probed at 526 nm. d) S5, probed at 540 nm. e) S5, probed at 575 nm. f) S300, probed at 540 nm.

cross sections are also affected by the different positions of the probe relative to the bandgap and uncertainties in the determination of the beam area.

Each average number of excitations in each QD ensemble, $\langle N \rangle$, that was extracted was in turn used to calculate the initial population of each exciton level using Eq. 1. There are three different sets of populations, one for the $\langle N \rangle$s from the upper-boundary fit ($\langle N \rangle_{max}$), one from the lower-boundary fit ($\langle N \rangle_{min}$) and one from the average fit ($\langle N \rangle_{avg}$), for each QD sample. As an example, the results for the L0 sample at the band edge are shown in Table S6, Table S7 and Table S8 respectively.

Table S6: Initial populations for sample L0 at 592 nm calculated from the upper-boundary fit

Intensity	$\langle N \rangle_{max}$	P_0	P_1	P_2	P_3	P_4	$P_5 + P_6 + ...$
$1.0 \cdot I_0$	0.062	0.940	0.058	0.002	–	–	–
$3.8 \cdot I_0$	0.238	0.788	0.188	0.022	0.002	–	–
$11.6 \cdot I_0$	0.723	0.486	0.351	0.127	0.031	0.001	0.001
$45.8 \cdot I_0$	2.843	0.058	0.166	0.235	0.223	0.159	0.090

Table S7: Initial populations for sample L0 at 592 nm calculated from the average values fit

Intensity	$\langle N \rangle_{avg}$	P_0	P_1	P_2	P_3	P_4	$P_5 + P_6 + ...$
$1.0 \cdot I_0$	0.065	0.937	0.061	0.002	–	–	–
$3.8 \cdot I_0$	0.251	0.778	0.195	0.025	0.002	–	–
$11.6 \cdot I_0$	0.761	0.467	0.356	0.135	0.034	0.001	0.001
$45.8 \cdot I_0$	2.995	0.050	0.150	0.224	0.224	0.184	0.101

Table S8: Initial populations for sample L0 at 592 nm calculated from the lower-boundary fit

Intensity	$\langle N \rangle_{min}$	P_0	P_1	P_2	P_3	P_4	$P_5 + P_6 + ...$
$1.0 \cdot I_0$	0.069	0.934	0.064	0.002	–	–	–
$3.8 \cdot I_0$	0.263	0.769	0.202	0.027	0.002	–	–
$11.6 \cdot I_0$	0.799	0.450	0.359	0.144	0.038	0.001	0.001
$45.8 \cdot I_0$	3.143	0.043	0.136	0.213	0.223	0.209	0.110

3. Extraction of the K_N coefficients

The time evolution of the populations in the different exciton levels in a five-level system are given by the following equations retrieved using chemical kinetics.[3]

$$\frac{dP_4(t)}{dt} = -k_4 \cdot P_4(t) \Rightarrow P_4(t) = P_4(0) \cdot e^{-k_4 \cdot t} \tag{S3.1a}$$

$$\frac{dP_3(t)}{dt} = k_4 \cdot P_4(t) - k_3 \cdot P_3(t) \Rightarrow P_3(t) = P_3(0) \cdot e^{-k_3 \cdot t} + P_4(0) \cdot \frac{k_4}{k_3 - k_4} \cdot (e^{-k_4 \cdot t} - e^{-k_3 \cdot t}) \tag{S3.1b}$$

$$\begin{aligned} \frac{dP_2(t)}{dt} =& k_3 \cdot P_3(t) - k_2 \cdot P_2(t) \Rightarrow \\ P_2(t) =& P_2(0) \cdot e^{-k_2 \cdot t} + P_3(0) \cdot \frac{k_3}{(k_2 - k_3)} \cdot \left(e^{-k_3 \cdot t} - e^{-k_2 \cdot t}\right) \\ &+ P_4(0) \cdot \left(\frac{k_4 \cdot k_3 \cdot e^{-k_4 \cdot t}}{(k_2 - k_4) \cdot (k_3 - k_4)} - \frac{k_4 \cdot k_3 \cdot e^{-k_3 \cdot t}}{(k_2 - k_3) \cdot (k_3 - k_4)} + \frac{k_4 \cdot k_3 \cdot e^{-k_2 \cdot t}}{(k_2 - k_3) \cdot (k_2 - k_4)} \right) \end{aligned} \tag{S3.1c}$$

$$\begin{aligned} \frac{dP_1(t)}{dt} =& k_2 \cdot P_2(t) - k_1 \cdot P_1(t) \Rightarrow \\ P_1(t) =& P_1(0) \cdot e^{-k_1 \cdot t} + P_2(0) \cdot \frac{k_2}{(k_1 - k_2)} \cdot \left(e^{-k_2 \cdot t} - e^{-k_1 \cdot t}\right) \\ &+ P_3(0) \cdot \left(\frac{k_3 \cdot k_2 \cdot e^{-k_3 \cdot t}}{(k_1 - k_3) \cdot (k_2 - k_3)} - \frac{k_3 \cdot k_2 \cdot e^{-k_2 \cdot t}}{(k_1 - k_2)(k_2 - k_3)} + \frac{k_3 \cdot k_2 \cdot e^{-k_1 \cdot t}}{(k_1 - k_2)(k_1 - k_3)} \right) \\ &+ P_4(0) \cdot \left(\frac{k_4 \cdot k_3 \cdot k_2 \cdot e^{-k_4 \cdot t}}{(k_1 - k_4) \cdot (k_2 - k_4) \cdot (k_3 - k_4)} - \frac{k_4 \cdot k_3 \cdot k_2 \cdot e^{-k_3 \cdot t}}{(k_1 - k_3) \cdot (k_2 - k_3) \cdot (k_3 - k_4)} \right) \\ &+ P_4(0) \cdot \left(\frac{k_4 \cdot k_3 \cdot k_2 \cdot e^{-k_2 \cdot t}}{(k_1 - k_2) \cdot (k_2 - k_3) \cdot (k_2 - k_4)} - \frac{k_4 \cdot k_3 \cdot k_2 \cdot e^{-k_1 \cdot t}}{(k_1 - k_2) \cdot (k_1 - k_3) \cdot (k_1 - k_4)} \right) \end{aligned} \tag{S3.1d}$$

According to Eq. 4 it is possible to write the total signal from the QDs as

$$S_{tot}(t) = K_1 \cdot P_1(t) + K_2 \cdot P_2(t) + K_3 \cdot P_3(t) + K_4 \cdot P_4(t). \tag{S3.2}$$

On the other hand, the fitting gives an equation of the form

$$S_{tot}(t) = A_{1,\alpha} \cdot e^{-k_{1,\alpha} \cdot t} + A_{1,\beta} \cdot e^{-k_{1,\beta} \cdot t} + A_2 \cdot e^{-k_2 \cdot t} + A_3 \cdot e^{-k_3 \cdot t} + A_4 \cdot e^{-k_4 \cdot t} \tag{S3.3}$$

To account for the biexponential single-exciton decay, we assume that there are two parallel decay channels, with $\alpha = A_{1,\alpha}/(A_{1,\alpha} + A_{1,\beta})$ of the total following the slow route and $\beta = 1 - \alpha$ following the fast route, the two routes being identical except that the rate constant of the single-exciton decay is $k_{1,\alpha}$ for the slow route but $k_{1,\beta}$ for the fast route. The signal from the slow route will be

$$S_{tot,\alpha}(t) = A_{1,\alpha} \cdot e^{-k_{1,\alpha} \cdot t} + \alpha \cdot (A_2 \cdot e^{-k_2 \cdot t} + A_3 \cdot e^{-k_3 \cdot t} + A_4 \cdot e^{-k_4 \cdot t}) \tag{S3.4}$$

and analogously, replacing α with β, for the fast route, with $S_{tot}(t) = S_{tot,\alpha}(t) + S_{tot,\beta}(t)$.

Eq. S3.1a–d and Eq. S3.2 are adapted to describe a specific channel by replacing k_1 with $k_{1,\alpha}$ ($k_{1,\beta}$) and K_N with $K_{N,\alpha}$ ($K_{N,\beta}$). In the following, we develop the argument for the slow route, but it holds, *mutatis mutandis*, equally for the fast route. The modified Eq. S3.2 can be rewritten on the same form as Eq. S3.4 by inserting the expressions for $P_N(t)$ given by the modified Eq. S3.1a–d, and collecting the occurrences of each exponential. The prefactors of the exponentials are then sums of up to four terms, each containing K_N times a coefficient. Setting the right-hand sides of Eq. S3.2 and Eq. S3.4 as equal shows that the prefactors on each side must be equal for the equality to hold, so we obtain a system of four equations that can be written on matrix form as

$$\mathbf{F}_\alpha \cdot \begin{pmatrix} K_{1,\alpha} \\ K_{2,\alpha} \\ K_{3,\alpha} \\ K_{4,\alpha} \end{pmatrix} = \begin{pmatrix} A_{1,\alpha} \\ A_2 \\ A_3 \\ A_4 \end{pmatrix}, \tag{S3.5}$$

where $\mathbf{F}_\alpha$ is a 4-by-4 matrix such that $F_{ij,\alpha}$ is the coefficient of $K_{j,\alpha} \cdot e^{-k_i \cdot t}$ ($K_{j,\alpha} \cdot e^{-k_{1,\alpha} \cdot t}$ for $F_{1j,\alpha}$) in the rewritten Eq. S3.2. This system can be solved for $K_{N,\alpha}$. Finally, K_N for the entire system is obtained through $K_N = K_{N,\alpha} + K_{N,\beta}$.

The different K_N coefficients were extracted from Eq. S3.5 separately for each intensity for all the samples, using the $P_N(0)$ calculated from each $\langle N \rangle$ fit, and for the populations from average ΔA_0 also for the maximum and minimum time constants in addition to the optimum. As an example, the K_N values for the L0 sample at the band edge are shown in Table S9, Table S10 and Table S11.

Table S9: The extracted K_N coefficients for sample L0 at 592 nm from the populations corresponding to $\langle N \rangle_{max}$

Intensity	K_1	K_2	K_3	K_4
$1.0 \cdot I_0$	-0.0190	-0.1734	$--$	$--$
$3.8 \cdot I_0$	-0.0224	-0.1049	-0.6843	$--$
$11.6 \cdot I_0$	-0.0233	-0.0863	-0.2260	-1.3906
$45.8 \cdot I_0$	-0.0241	-0.0593	-0.1464	-0.2433

Table S10: The extracted K_N coefficients for sample L0 at 592 nm from the populations corresponding to $\langle N \rangle_{avg}$

Intensity	K_1	K_2	K_3	K_4
$1.0 \cdot I_0$	-0.018	-0.157	$--$	$--$
$3.8 \cdot I_0$	-0.021	-0.096	-0.597	$--$
$11.6 \cdot I_0$	-0.023	-0.081	-0.204	-1.179
$45.8 \cdot I_0$	-0.024	-0.058	-0.139	-0.228

Table S11: The extracted K_N coefficients for sample L0 at 592 nm from the populations corresponding to $\langle N \rangle_{min}$

Intensity	K_1	K_2	K_3	K_4
$1.0 \cdot I_0$	-0.017	-0.144	$--$	$--$
$3.8 \cdot I_0$	-0.021	-0.089	-0.526	$--$
$11.6 \cdot I_0$	-0.022	-0.076	-0.185	-1.016
$45.8 \cdot I_0$	-0.024	-0.057	-0.134	-0.215

4. Cross section for stimulated emission[4]

The oscillator strength of a transition, f_{21}, is related to the Einstein coefficient for spontaneous emission, A_{21}, according to

$$f_{21} = -\frac{1}{3} \cdot A_{21} \cdot \gamma_{cl} \quad \text{where} \quad \gamma_{cl} = \frac{e^2 \cdot \omega_{21}^2}{6\pi \cdot \epsilon_0 \cdot m \cdot c^3} \tag{S4.1}$$

and ω_{21} is the oscillation frequency. The Einstein coefficient for spontaneous emission can be calculated from

$$A_{21} = \frac{1}{t_{sp}} \tag{S4.2}$$

where t_{sp} is the radiative lifetime of the upper level. The cross section for stimulated emission is given by

$$\sigma_{st}(\nu) = f_{21} \cdot g(\nu) \tag{S4.3}$$

where $g(\nu)$ is the spectral line shape function which is given by

$$g(\nu) = \frac{\pi \cdot e^2}{(\nu - \nu_0)^2 \cdot \Delta\nu_{FWHM} \cdot \pi^2 \cdot 2 \cdot \epsilon_0 \cdot m \cdot c}. \tag{S4.4}$$

Using the radiative lifetime extracted from the fluorescence quantum yield and the fluorescence lifetime, we could estimate that $\sigma_{st} \approx 0.02 \cdot \sigma_{abs}$, where σ_{st} is the cross section for stimulated emission.

5. Absorption cross sections from different pump intensities

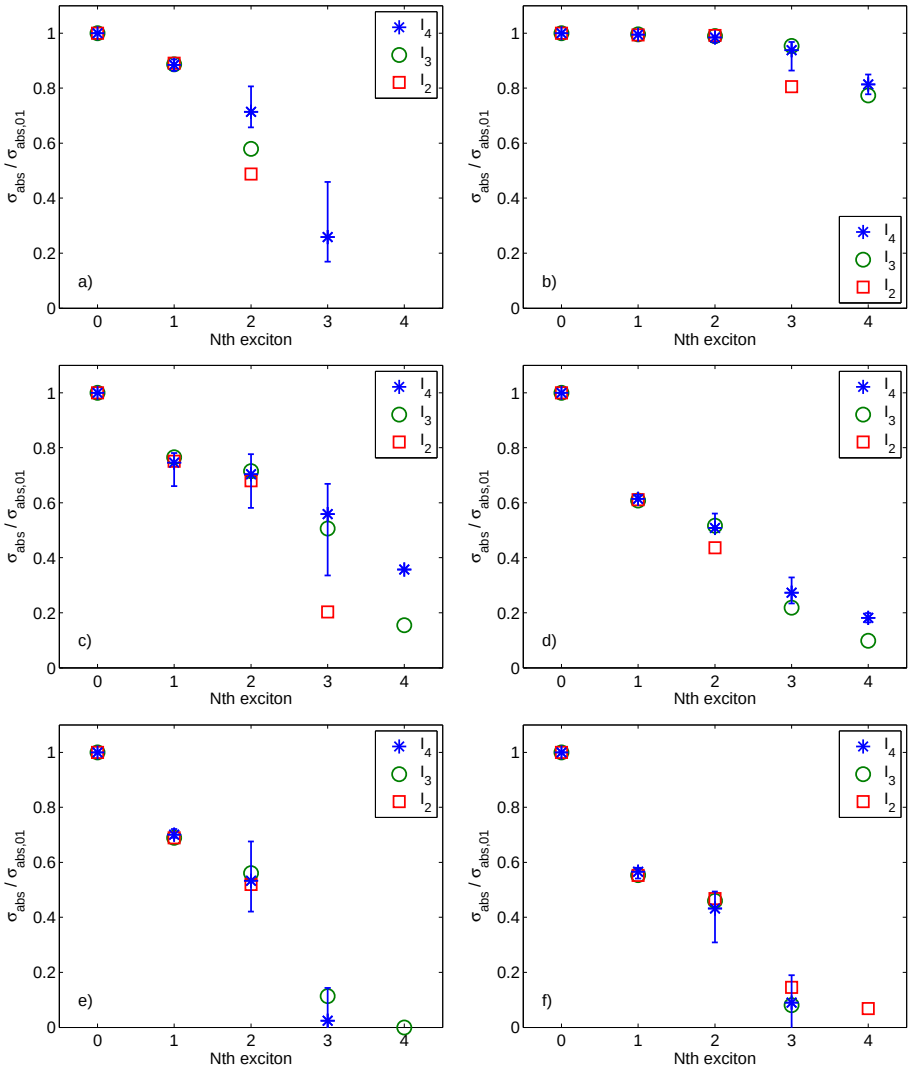

Figure S3: Relative absorption cross sections for $N \rightarrow N + 1$-exciton transitions in sample L0 probed at 592 nm (a), L0 probed at 550 nm (b), S0 probed at 526 nm (c), S5 probed at 540 nm (d), S5 probed at 575 nm (e) and S300 probed at 540 nm (f), calculated from three different pump intensities. The error bars for I_4 were calculated by repeating the fitting procedure with the time constants fixed at their maximum (minimum) values as estimated from a semilogarithmic plot.

References

(1) Yu, W.; Qu, L.; Guo, W.; Peng, X. Experimental Determination of the Extinction Coefficient of CdTe, CdSe, and CdS Nanocrystals. *Chemistry of Materials* **2003**, *15*,

2854–2860.

(2) Leatherdale, C. A.; Woo, W.-K.; Mikulec, F. V.; Bawendi, M. G. On the Absorption Cross Section of CdSe Nanocrystal Quantum Dots. *J. Phys. Chem. B* **2002**, *106*, 7619–7622.

(3) Hill Jr, C. G. *An Introduction to Chemical Engineering Kinetics and Reactor Design*, 1st ed.; John Wiley and Sons: New York, 1977; Chapter 5.3.

(4) Hilborn, R. C. Einstein Coefficients, Cross Sections, f Values, Dipole Moments, and All That. *Am. J. Phys.* **1982**, *50*, 982–986.